Comparative Study of High-speed Permanent Magnet Synchronous Motors with In-line Slot Conductors and Equidirectional Toroidal Windings

Yinjun Sun[1], Peixin Wang[1], Rui Nie[1], Fuquan Nie[2], Peng Gao[3], and Jikai Si[1]

[1]Department of Electrical and Information Engineering
Zhengzhou University, Zhengzhou 450001, China
syjxixinyidian163.com, wangpeixin509@126.com, nierui@zzu.edu.cn, sijikai527@126.com

[2]Department of Henan Institute of Science and Technology
Xinxiang, Henan 453000, China
976028398@qq.com

[3]Department of Henan United Electric Power Technology Co. Ltd.
Zhengzhou 450001, China
15290418261@qq.com

***Abstract* –** The high-speed permanent magnet synchronous motor (HSPMSM) plays an important role in a wide range of engineering fields due to its high power density, high efficiency, and light weight. In this paper, a HSPMSM equipped with in-line slot conductors (I-LSC) is proposed and compared with one equipped with equidirectional toroidal winding (ETW). Firstly, the differences between them are revealed, including topology, back-electromotive force (EMF), slot fill factor, copper loss, and torque. Secondly, two-dimensional finite element method (2D-FEM) tools are used to obtain more precise performance such as air-gap field, back-EMF, torque characteristics, efficiency maps, and the unbalanced magnetic force (UMF). Considering the end-windings of copper loss of ETW and the end ring copper loss of I-LSC, the losses and efficiency of two motors are simulated by three-dimensional finite element method (3D-FEM). Finally, the simulation results validate the feasibility of the newly proposed winding and indicate that in-line slot conductors have superiority in power density due to the high slot fill factor.

***Index Terms* –** Equidirectional toroidal winding, high fill factor, high-speed permanent magnet synchronous motor, in-line slot conductor, power density.

I. INTRODUCTION

The demands for high-speed (HS) motor technologies are continuously evolving, with a focus on achieving high power density, enhanced efficiency, and energy conservation in the engineering applications such as automobiles, aircraft, and flywheel energy storage [1–3]. According to the operation principle, they can principally be divided into HS switched reluctance, induction, and permanent magnet synchronous motors [3–5]. Notably, high-speed permanent magnet synchronous motors (HSPMSM) with diverse stator and rotor structures stand out for their exceptional performance. HSPMSMs not only demonstrate remarkable efficiency and power density but also boast a broader range of applications and quicker dynamic response capabilities. Hence, HSPMSM can be a good candidate in the HS application field [6].

In the past few decades, the motor has been vigorously researched and promoted to seek the maximize power density, which put very high requirements on the design of the rotor/stator [6, 7]. The influence of the rotor structure on power density has been emphasized previously [8]. Another important factor for power density is the stator winding. For example, the fractional slot concentrated windings (FSCW) in conventional permanent magnet (PM) motors possess high power density while the multiphase motors with integral slot distributed windings can offer much higher torque than the FSCW [9]. The motor end-windings should be designed shorter, otherwise excessive axial length leads to low torque density as outlined in [10]. HSPMSMs with hairpin structures can have high torque but the slot shape is always parallel as demonstrated in [11]. Here follows an overview concerning diverse windings.

HSPMSM generally can be configured with [12]:

(1) overlapping windings: Fig. 1 (a) is a representative example that uses a full pitch overlapping windings with six slots [13]. Hence, HSPMSM with overlapping windings have a relatively high winding factor. However, regardless of the single layer and double layer, these overlapping windings need to be set

Submitted On: November 8, 2023
Accepted On: July 23, 2024
https://doi.org/10.13052/2024.ACES.J.390610

up in a crisscross arrangement, which makes the motor not only display bulk end-windings but also increases copper consumption. Moreover, the end-windings result in a long axial length with a consequent reduction in power density [13].

(2) Non-overlapping windings sometimes can be involved in concentrated windings, such as tooth-wound and yoke-wound. Compared with overlapping windings, tooth-wound windings have the advantage of short end-windings, low copper loss, and shorter motor axial length [14]. As depicted in Figs. 1 (b) and (c), single-layer and double-layer windings are sleeve windings that have been extensively utilized in permanent magnet motors. Taking 3s2p as an example, the winding factor for Figs. 1 (b) and (c) is 0.866 [15–17]. Halbach winding is also a type of non-overlapping winding, which can achieve the effect of enhancing and weakening the magnetic field on one side in PMs. But the winding factor is also 0.866 [18]. The equidirectional toroidal windings (ETW) are subordinate to yoke-wound windings and have been proven to have a conductor factor of 1 [19]. Furthermore, the utilization rate of windings has been improved by utilizing a dual-rotor structure to address end-winding [20]. ETW can significantly enhance torque density in various types of motors, such as axial flux PMs, radial flux PMs, and linear motors [21–23]. However, single rotor radial flux PMs with ETW has the disadvantage of low winding utilization rate [24]. Hence, the new topology, the in-line slot conductor (I-LSC), is envisaged and proposed in this paper. In this way, this type of winding can be seen as the ETW where the end-windings are omitted, and the myriads of winding conductors are infinitely approximated to a whole conductor that is placed in the stator slot in Fig. 1 (d). The I-LSC can improve winding utilization and have a high slot fill factor in a single rotor motor. Besides crucial merits, I-LSC can reduce copper consumption. It can be predicted to be suitable for HS motors due to the low number of turns. The influence of ETW configuration has been studied on HS operation but I-LSC has not been systematically investigated [25].

The major objective of this paper is to evaluate and confirm the merits and demerits of the new proposed I-LSC and the existing ETW in HSPMSM by a fair comparison. The constructions and operation principles of I-LSC and ETW are introduced in Section II. Then, the main performance of similarities and differences between the two motors is revealed in Section III. Finally, a summary of this paper as well as directions for future research work are presented in Section IV.

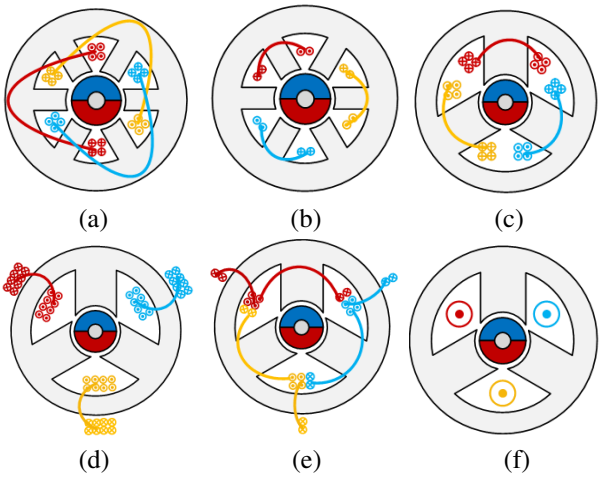

Fig. 1. Various winding types: (a) distributed winding, (b) single layer winding, (c) double layer winding, (d) ETW, (e) Halbach winding, and (f) I-LSC.

II. STRUCTURE AND OPERATION PRINCIPLES

The construction of the mentioned motor with ETW and the proposed motor with I-LSC are named ETW-HSPMSM and I-LSC-HSPMSM, respectively, as shown in Fig. 2. What they have in common is the 3s2p topologies to reduce the operating frequency and minimize switching losses. The same rotors are external-installed with PMs (N30SH) which can be diametrically magnetized. Furthermore, all other parameters are the same for comparison purposes, except that ETW-HSPMSM has more outer teeth and end-windings than I-LSC-HSPMSM.

A. Structure

The differences between the two motors are mainly on the stator side. Firstly, the two stators have similar inside teeth and slots. However, ETW-HSPMSM is equipped with external teeth to place the outside conductors, as shown in Fig. 2. Secondly, the windings of ETW-HSPMSM are wound around the stator yoke but I-

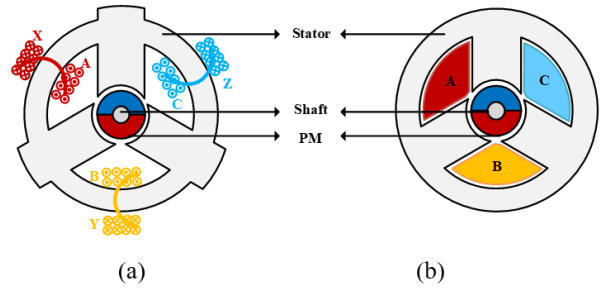

Fig. 2. 3s2p motor topology: (a) ETW-HSPMSM and (b) I-LSC-HSPMSM.

LSC-HSPMSM is inserted into the stator slots. In addition, the positive sides (A, B, and C) of the ETW are positioned inside the stator core, while the negative sides (X, Y, and Z) are situated on the outside, as illustrated in Fig. 2 (a). Only the positive sides (A, B, and C) can be considered as effective edges. However, I-LSC only has the positive sides (A, B, and C) without negative sides. In ETW-HSPMSM, the incoming line terminals (A, B, and C) need to be linked to a three-phase power source, while the outgoing terminals (X, Y, and Z) are connected together by a wye configuration. Conversely, for I-LSC-HSPMSM, solid copper blocks (A, B, and C) are inserted into the stator slots and connected to the end ring. By contrast, there are no end-windings for I-LSC which reduces the invalid length to diminish the size of I-LSC-HSPMSM. The shape of the conductor can be made even closer to the shape of the slot to improve the slot fill factor.

B. Operation principle

To illustrate the operation principle of HSPMSMs with ETW and I-LSC clearly, it is analyzed by using the minimum unit motor as an example. Two motors are shown to be fed square wave currents to maintain consistency, which ETW had been reported in [20]. It is necessary to observe the operating principles of the two motors for their subsequent performance analysis. In Fig. 3, two motors are excited by the square wave current source, and the current during this period of one electrical cycle is divided into six intervals, each corresponding to specific three-phase current directions, as displayed in Table 1.

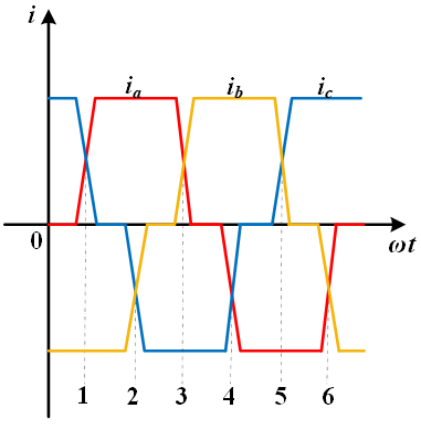

Fig. 3. Three-phase square waveform current.

The notation '+' denotes current outflow the plane of windings, while '-' signifies current inflow the plane, as indicated in Table 1. The current through the windings of ETW-HSPMSM and I-LSC-HSPMSM in a period will generate an armature magnetic field. The armature magnetic field rotates periodically with time and forms a periodical rotating magnetic field. Under the effect of the rotating magnetic field, the rotor core subsequently rotates. The armature magnetic field of two motors at three moments in sequence is selected successively to compare its distribution of magnetic field lines with the armature magnetic field at moment 0 in Fig. 4. Each time elapsed, N or S will undergo a counterclockwise rotation of 120 degrees. Thus, the armature magnetic field alternates in a periodic manner, forming a pair of poles.

Table 1: Three-phase winding current directions at different times

Current	Times						
	0	1	2	3	4	5	6
i_a	0	+	+	+	-	-	-
i_b	-	-	-	+	+	+	-
i_c	+	+	-	-	-	+	+

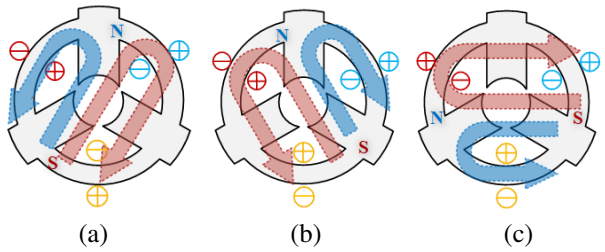

Fig. 4. Armature reaction field of ETW-HSPMSM: (a) time 2, (b) time 3, and (c) time 4.

Figure 5 demonstrates that the armature magnetic field of I-LSC-HSPMSM rotates counterclockwise which exhibits the same rotational direction as ETW-HSPMSM. However, ETW-HSPMSM has an effect of magnetic leakage because of the existence of end-windings.

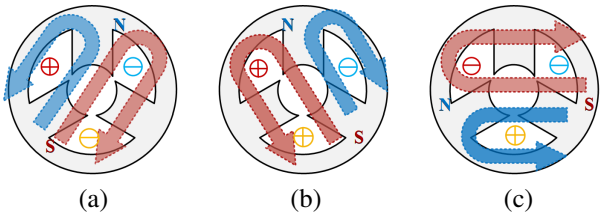

Fig. 5. Armature reaction field of I-LSC-HSPMSM: (a) time 2, (b) time 3, and (c) time 4.

The structure and materials of the PMs of the two motors are identical, and the parallel direction are all magnetized uniformly. Thus, the flux distribution generated by the PMs in both motors is identical. Consequently, this ensures that the magnetic load of the two

motors is identical, enabling a fairer comparison of their performance in subsequent analyses.

C. No-load back-EMF

The no-load back-electromotive force (EMF) is generated when the external rotor permanent magnet rotates around the Z-axis. Only the phase-EMF of positive sides (E_A, E_B, and E_C) are effective edges for the two motors due to the unique coil arrangement of ETW and I-LSC. The pitch factor (k_p) is the coefficient of reduction in the phase-EMF, which is always 0.5 [19]. The winding distributed coefficients (k_d) of the two motors are 1. The fundamental EMF component is E_0, which is given by:

$$E_0 = 2.22 f N_s \Phi_1, \tag{1}$$

where N_s is the number of turns per phase, f is the motor frequency, and ϕ_1 is the fundamental flux generated by PM at each pole.

For ETW-HSPMSM and I-LSC-HSPMSM, E_0 is proportional to the number of turns and the fundamental flux.

D. Fill factor

According to stator tooth width and yoke height, the cross-sectional area of stator slot and conductor (A_{cond}) can be determined for slot fill factor. A high slot fill factor (k_{fill}) decreases the motor volume by reducing the unnecessary area of the slot, which can be calculated by:

$$k_{fill} = \frac{A_{cond} N_s}{S_{slot}}, \tag{2}$$

where A_{cond} is the cross-sectional area of one conductor while S_{slot} is the stator slot.

I-LSC has arranged the winding as close to the slot shape as feasible after removing the thickness of the insulating paper. However, for ETW, there will be a gap between the round-copper wires no matter how they are placed.

E. Torque

The electromagnetic torque on the rotor in a synthetic magnetic field can be expressed as:

$$T_e = \frac{2.22 m f N_s \Phi_1 I_{RMS} \cos\Phi_0 \eta}{2\pi f}, \tag{3}$$

where m is the phase number of the motor, Φ_0 is the angle formed by the current and back-EMF, and η is the efficiency of the motor.

The current per phase (I_{RMS}) is affected by current density (J_s). When stator slot area (S_{slot}) is determined, slot fill factor is also a principal element to affects I_{RMS}, which is given by:

$$I_{RMS} = J_s A_{cond}, \tag{4}$$

$$I_{RMS} = J_s \frac{S_{slot} k_{fill}}{N_s}. \tag{5}$$

Torque can be also expressed as:

$$T_e = 1.11 m B_g l_a D_{air} J_s k_{fill} S_{slot} \eta, \tag{6}$$

where l_a is stator active length, D_{air} is average value of the sum of the stator inner and outer diameters, and B_g is peak value of air-gap flux density. According to the above equation, if the mechanical structure of the motors and the materials of the PMs are determined, the torque will be proportional to the slot fill factor (k_{fill}) under the same current density.

F. Copper loss

Total copper loss (P_{TCL}) includes DC loss (P_{DC}) and AC loss (P_{AC}) [26]. In calculating DC copper loss, the end-windings of the ETW in the out slot should be taken into account in copper loss, while I-LSC has only one effective edge, which is given by:

$$P_{TCL} = P_{AC} + P_{DC}, \tag{7}$$

$$P_{DC} = 3\rho_{cu} I^2_{RMS} \frac{2(l_a + h_{sy}) N_s}{A_{cond}}, \tag{8}$$

where ρ_{cu} is the resistivity of copper, N_s is the number of in-series turns per phase, and h_{sy} is stator yoke height.

To verify the rationality of the proposed motor with I-LSC, the common and distinct characteristics of I-LSC-HSPMSM and ETW-HSPMSM are compared. At the same time, it is demonstrated that I-LSC-HSPMSM will have a higher torque than ETW-HSPMSM due to high slot fill factor. Moreover, due to its smaller volume, I-LSC-HSPMSM has a higher power density compared to ETW-HSPMSM. The following section will verify these conclusions by two-dimensional finite element method (2D-FEM) and three-dimensional finite element method (3D-FEM). Designing the two motors requires adhering to specific preconditions and constraints to ensure a fair comparison.

(1) Both motors possess identical dimensions and materials of the stators, PMs, and rotors. Magnetizing direction of PMs in both motors is identical.

Table 2: Optimized design parameters for two HSPMSM

	ETW-HSPMSM	**I-LSC-HSPMSM**
Stator out diameter D_0(mm)	54	54
Stator inner diameter D_i(mm)	16.2	16.2
Stator active length l_a(mm)	9.1	9.1
Air-gap length l_g(mm)	1.25	1.25
Shaft radius R_{shaft}(mm)	0.3	0.3
Number of series turns per phase N_s	36	1
Outer tooth height h_{ot}(mm)	3.3	0
Stator yoke height h_{sy}(mm)	6.3	6.3
Inner tooth width w_{it}(mm)	12.5	12.5
Current density J_s(mm)	9.7	9.7
Rated speed (krpm)	110	110
DC copper loss P_{dc}	6.78	2.65

(2) Air-gap length remains consistent between the two motors.

(3) The two motors are excited by the same current density. Based on these principles, the primary parameters of the two motors are presented in Table 2 [27].

III. ELECTROMAGNETIC CHARACTERISTICS OF TWO MOTORS

Each motor, ETW-HSPMSM and I-LSC-HSPMSM, is composed of a three-phase winding and a pair of magnets as its minimum unit. According to the aforementioned parameters and analysis, the electromagnetic performance of ETW-HSPMSM is consistent with what is presented in [25] firstly. It will be seen that there are some common points and differences in the electromagnetic performance by considering both no-load and on-load situations, respectively.

A. Air-gap flux density

The waveforms of air-gap flux density produced by two PMs of both motors exhibit similarity as depicted in Fig. 6 (a), which is due to the fact that the two motors ensure the same magnetic load conditions. It demonstrates that the outer teeth do not affect the air gap magnetic density. In Fig. 6 (b), it is illustrated that the amplitudes of the fundamental harmonic of the air-gap flux density in both motors are 0.85 T, with total harmonic distortions (THD) of 7.01% for each.

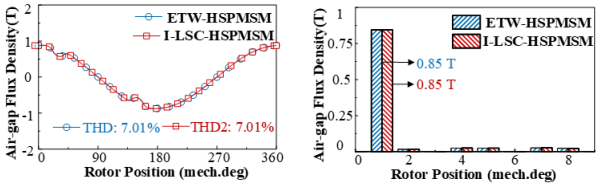

(a) (b)

Fig. 6. Air-gap flux density of ETW-HSPMSM and I-LSC-HSPMSM: (a) waveforms and (b) harmonic spectra.

B. Open-circuit flux linkage

The detailed flux density distribution of the two motors at the same rated speed of 110 krpm is depicted in Fig. 7, and the peak flux density is specifically located at the tip of the stator teeth. The flux linkage waveforms are shown in Fig. 8 (a), the peak value of ETW-HSPMSM is 2.0 mWb while I-LSC-HSPMSM is 0.056 mWb. There is an apparent difference in amplitudes for the two motors which can be mainly attributed to the different turns. The number of turns for ETW is 36 whereas I-LSC is only 1. The ratio of the maximum values of the flux linkage between the two motors is equal to the ratio of their respective numbers of turns. It is worth noting that the fundamental amplitude of ETW-HSPMSM is 2.32 mWb while I-LSC-HSPMSM is 0.05 mWb.

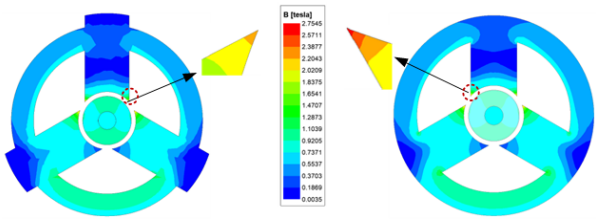

(a) (b)

Fig. 7. Equal potential and flux distributions of high-speed motors: (a) ETW-HSPMSM and (b) I-LSC-HSPMSM.

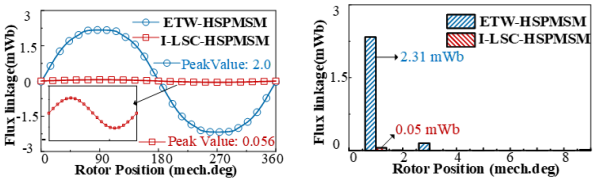

(a) (b)

Fig. 8. Flux linkage and its harmonic spectra of ETW-HSPMSM and I-LSC-HSPMSM: (a) waveforms and (b) harmonic spectra.

C. Back-EMF

The no-load back-EMF of the two motors with the rated speed of 110 krmp is shown in Fig. 9. It is evident that the peak values of no-load back-EMF in ETW-HSPMSM and I-LSC-HSPMSM are 24.52 V and 0.66 V, respectively. The basic harmonic amplitude of ETW-HSPMSM is 26 V, while that of I-LSC-HSPMSM is 0.63 V, which is shown in Fig. 9 (b). I-LSC-HSPMSM has 36 times lower back-EMF than ETW-HSPMSM because the number of turns is 36 times less than ETW-HSPMSM according to equation (1). THD of ETW-HSPMSM and I-LSC-HSPMSM is 3.84% and 0.24%, respectively. In particular, the 3rd harmonic of the phase back-EMF in both motors cannot be ignored. However, this 3rd harmonic is effectively eliminated in the line back-EMF, as illustrated in Fig. 10.

D. Armature reaction fields

Figure 11 illustrates the windings armature field of the two motors when subjected to square wave excitation under identical current density. I_{RMS} of I-LSC-HSPMSM is 576.1 A, and that of ETW-HSPMSM is 12.02 A. I-LSC has 1 turn while ETW has 36 turns. Peak value of I-LSC-HSPMSM is 0.151 T while peak value of ETW-HSPMSM is 0.114 T as shown in Fig. 11 (a).

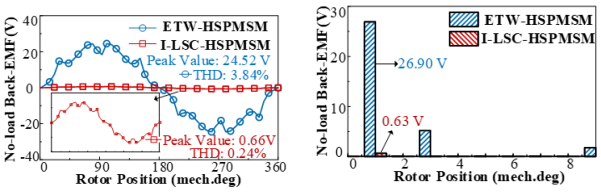

(a) (b)

Fig. 9. No-load back-EMF and its harmonic spectra of ETW-HSPMSM and I-LSC-HSPMSM: (a) waveforms and (b) harmonic spectra.

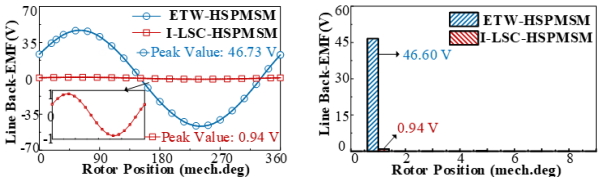

(a) (b)

Fig. 10. No-load line back-EMF of ETW-HSPMSM and I-LSC-HSPMSM: (a) waveforms and (b) harmonic spectra.

Therefore, the ratio of peak values of the armature magnetic fields of the two motors is approximately equal to the ratio of the incoming current of the two motors. In Fig. 11 (b), the main fundamental values of ETW-HSPMSM and I-LSC-HSPMSM are 0.05 T and 0.072 T, respectively.

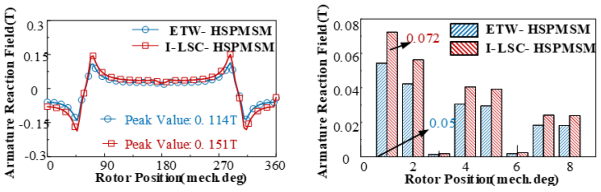

(a) (b)

Fig. 11. Armature field of ETW-HSPMSM and I-LSC-HSPMSM: (a) waveforms and (b) harmonic spectra.

E. On-load torque characteristics

With a conductor cross-sectional area of 1.24 mm^2 and a slot area cross-sectional of 73.50 mm^2, ETW-HSPMSM can theoretically achieve a maximum slot fill factor of 60.71%. As for I-LSC-HSPMSM, the winding shape is close to the stator slot and k_{fill} of I-LSC can extend up to 80.00%. Under square-wave excitation with the same current density, the average torque of the two motors is 47.84 mNm and 63.52 mNm, respectively, demonstrated in Fig. 12. It can be observed that the torque ratio of the two motors and the slot fill factor ratio are the same. The output torque of I-LSC-HSPMSM is 24.68% higher than that of ETW-HSPMSM. Meanwhile, torque ripple is 1.30% lower than that of ETW-HSPMSM.

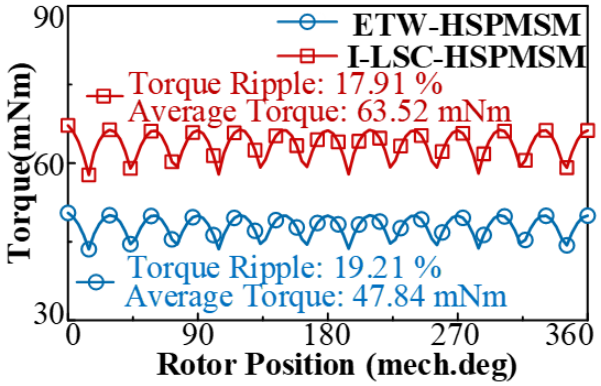

Fig. 12. Torque waveforms of ETW-HSPMSM and I-LSC-HSPMSM under rated load conditions.

F. Loss and efficiency map

In HSPMSMs, the main losses are stator iron loss and copper loss. The application of 3D-FEM can be applied for a more comprehensive analysis of motor losses, including the calculation of the losses of end-windings. Iron loss accounts for the main component of total loss due to the high frequency of the HSPMSM, which is shown in Fig. 13. Copper loss is obtained by integrating the current density over one electrical cycle for both motors. AC loss is determined by subtracting the calculated DC copper loss from this total loss.

Two motors have different losses due to the different currents which are fed into the windings at the same current density. Iron core loss of ETW-HSPMSM is 88.5 W, while that of I-LSC-HSPMSM is 76.4 W. I-LSC-HSPMSM has a larger cross-sectional area of the conductor and lower resistance, resulting in DC

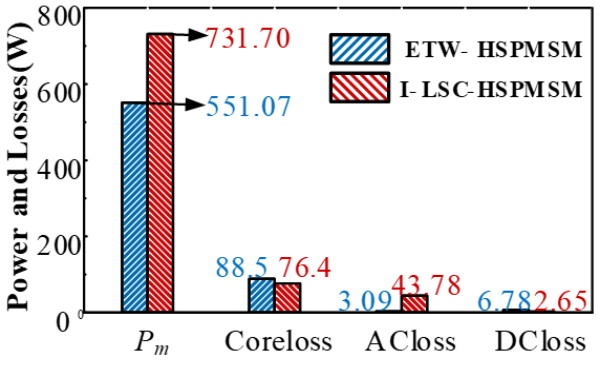

Fig. 13. Comparison of on-load losses at rated speeds.

loss of 2.65 W compared to ETW-HSPMSM's DC loss of 6.78 W. It is worth mentioning that AC loss of I-LSC-HSPMSM reaches 43.78 W due to the skin effect, whereas AC loss of ETW-HSPMSM is only 3.09 W. At high frequencies, AC copper loss of I-LSC-HSPMSM is high because of the skin effect. According to equation (9), output power of ETW-HSPMSM is 551.07 W, while that of I-LSC-HSPMSM is 731.70 W (see Fig. 13). However, the efficiency of ETW-HSPMSM is 84.85%, and that of I-LSC-HSPMSM is 85.63%, as calculated by equation (10):

$$P_m = T_e \frac{2\pi n}{60}, \tag{9}$$

$$\eta = \frac{P_{\mathrm{m}}}{P_{\mathrm{m}} + P_{AC} + P_{\mathrm{core}} + P_{DC}} \times 100\%, \tag{10}$$

where P_m is the output mechanical power, P_{core} is the stator core loss, and n is the rated speed.

The output torque will be affected because of different excitations. Under sinusoidal excitation, the output torque is 9% smaller than the square wave excitation. The efficiency map should be generated under the sinusoidal excitation as shown in Fig. 14.

When the two motors are in the bus voltage of 35.04 V and the current density is 0-12 J/mm^2, the highest efficiency of both motors is 85.02%. Under the same current density, the output torque of I-LSC-HSPMSM is still higher than that of ETW-HSPMSM. Core loss of the two motors increases much faster than the increment of the output power, which leads to a high-efficiency area not at the point of inflection. However, in the range of 200 krmp, output torque of I-LSC-HSPMSM only declines by 7.82%, while ETW-HSPMSM drops to 49.39% at 200 krmp. Therefore, I-LSCHSPMSMs are more suitable for high-speed applications than ETW-HSPMSMs.

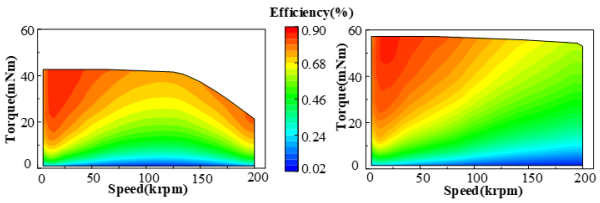

(a) (b)

Fig. 14. Efficiency map of two motors: (a) ETW-HSPMSM and (b) I-LSC-HSPMSM.

G. Unbalanced magnetic force

In addition to output power, unbalanced magnetic force (UMF) is also an important performance index for HS operation. UMF significantly affects vibration, noise level, and life of bearings, which can be calculated by [28]:

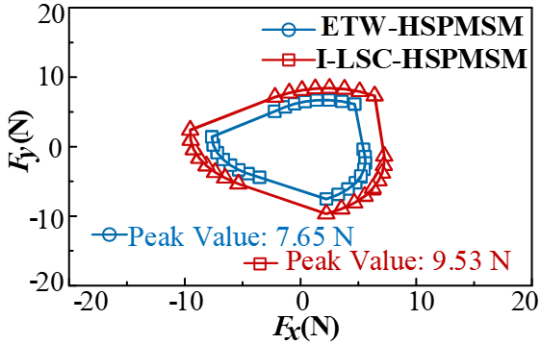

Fig. 15. Orthogonal components of unbalanced magnetic force.

$$F_x = \frac{r_{ag} l_a}{2\mu_0} \int_0^{2\pi} [(B_t^2 - B_r^2)\cos\theta + 2B_r B_t \sin\theta] d\theta, \tag{11}$$

$$F_y = \frac{r_{ag} l_a}{2\mu_0} \int_0^{2\pi} [(B_t^2 - B_r^2)\cos\theta - 2B_r B_t \sin\theta] d\theta, \tag{12}$$

where F_x and F_y are two orthogonal components of UMF, r_{ag} is radius of the air-gap, μ_0 is permeability of a vacuum, and B_r and B_t are radial and tangential components of air-gap flux density.

No matter the ETW and I-LSC, they both have the UFM shown in Fig. 15. Maximum value of ETW-HSPMSM is 7.65 N and of I-LSC-HSPMSM is 9.53 N. UMF will appear in the 3s2p motors at rated high speed due to asymmetric stator structure. Therefore, future work should change the pole-slot combination to offset UMF.

IV. CONCLUSION

In this paper, an HSPMSM with I-LSC is proposed and compared with ETW. It can be seen that the proposed motor (I-LSC-HSPMSM) has superiority in output torque due to a high slot fill factor at the same speed. Comparative studies on the two motors also show that the power density of I-LSC-HSPMSM is higher than ETW-HSPMSM due to high power and small volume. Compared with ETW, the I-LSC can be an excellent choice in HS motors from the point of maintaining a high torque at high speed. Moreover, I-LSC-HSPMSM has the advantages of dealing with the problem of the end-windings of ETW in the radial motor. However, I-LSC-HSPMSM inevitably has higher AC loss at high speeds due to skin effects. It can be concluded that I-LSC has a bright future and new challenges which should be solved in HS applications. As for unbalanced magnetic force, it can be known that the two motors both exist, which will be investigated in future studies for an appropriate structure. Subsequently, a motor prototype will be fabricated to verify the correctness of the ideas and simulations.

ACKNOWLEDGMENT

This work was supported by the National Natural Science Foundation of China under Grant 52307070, 52277069, and 52207067, the Postdoctoral Fellowship Program of China Postdoctoral Science Foundation under Grant GZC20232386, and the Major Special Project for Collaborative Innovation in Zhengzhou under Grant 20XTZX12023, and the Henan Province Key R&D and promotion projects under Grant 232102221016.

REFERENCES

[1] C.-W. Lin, J. F. Tu, and J. Kamman, "An integrated thermo-mechanical-dynamic model to characterize motorized machine tool spindles during very high speed rotation," *International Journal of Machine Tools and Manufacture,* vol. 43, no. 10, pp. 1035-1050, 2003.

[2] D. J. Tao, K. L. Zhou, F. Lv, Q. P. Dou, J. X. Wu, Y. T. Sun, and J. B. Zou, "Magnetic field characteristics and stator core losses of high-speed permanent magnet synchronous motors," *Energies,* vol. 13, no. 3, Feb. 2020.

[3] D. Gerada, A. Mebarki, N. L. Brown, C. Gerada, A. Cavagnino, and A. Boglietti, "High-speed electrical machines: Technologies, trends, and developments," *IEEE Transactions on Industrial Electronics,* vol. 61, no. 6, pp. 2946-2959, June 2014.

[4] G. Buticchi, D. Gerada, L. Alberti, M. Galea, P. Wheeler, S. Bozhko, S. Peresada, H. Zhang, C. M. Zhang, and C. Gerada, "Challenges of the optimization of a high-speed induction machine for naval applications," *Energies,* vol. 12, no. 12, June 2019.

[5] N. Bianchi, S. Bolognani, and F. Luise, "Potentials and limits of high-speed PM motors," *IEEE Transactions on Industry Applications,* vol. 40, no. 6, pp. 1570-1578, Nov.-Dec. 2004.

[6] A. Toba and T. A. Lipo, "Generic torque-maximizing design methodology of surface permanent-magnet vernier machine," *IEEE Transactions on Industry Applications,* vol. 36, no. 6, pp. 1539-1546, Nov.-Dec. 2000.

[7] G. Liu, Y. Wang, X. Xu, W. Ming, and X. Zhang, "The optimal design of real time control precision of planar motor," *The Applied Computational Electromagnetics Society Journal (ACES),* vol. 32, no. 10, pp. 948-954, Oct. 2017.

[8] M. Kimiabeigi, R. Long, J. D. Widmer, and Y. Gao, "Comparative assessment of single piece and fir-tree-based spoke type rotor designs for low-cost electric vehicle application," *IEEE Transactions on Energy Conversion,* vol. 32, no. 2, pp. 486-494, June 2017.

[9] L. Xu, G. Liu, W. Zhao, J. Ji, H. Zhou, W. Zhao, and T. Jiang, "Quantitative comparison of integral and fractional slot permanent magnet vernier motors," *IEEE Transactions on Energy Conversion,* vol. 30, no. 4, pp. 1483-1495, 2015.

[10] T. R. He, Z. Q. Zhu, F. Xu, H. Bin, D. Wu, L. M. Gong, and J. T. Chen, "Comparative study of 6-slot/2-pole high-speed permanent magnet motors with different winding configurations," *IEEE Transactions on Industry Applications,* vol. 57, no. 6, pp. 5864-5875, 2021.

[11] S. Balasubramanian, N. Langmaack, and M. Henke, "Evaluation and loss estimation of a high-speed permanent magnet synchronous machine with hairpin windings for high-volume fuel cell applications," *Elektrotechnik und Informationstechnik,* vol. 138, no. 6, pp. 415-423, Oct. 2021.

[12] T. He, Z. Q. Zhu, F. Xu, Y. Wang, H. Bin, and L. Gong, "Electromagnetic performance analysis of 6-slot/2-pole high-speed permanent magnet motors with coil-pitch of two slot-pitches," *IEEE Transactions on Energy Conversion,* vol. 37, no. 2, pp. 1335-1345, June 2022.

[13] M. Merdzan, J. J. H. Paulides, and E. A. Lomonova, "Comparative analysis of rotor losses in high-speed permanent magnet machines with different winding configurations considering the influence of the inverter PWM," in *2015 Tenth International Conference on Ecological Vehicles and Renewable Energies (EVER),* 2015.

[14] Z. Q. Zhu, Z. Y. Zhao, Y. W. Liu, F. R. Liang, D. W. Huang, and H. L. Liu, "Effect of end-winding on electromagnetic performance of fractional slot and Vernier PM machines with different slot/pole number combinations and winding configurations," *IEEE Access,* vol. 10, pp. 49934-49955, 2022.

[15] Y. Xu, Z. Xu, H. Wang, and W. Liu, "Research on magnetic-fluid-thermal-stress multi-field bidirectional coupling of high speed permanent magnet synchronous motors," *Case Studies in Thermal Engineering,* vol. 54, Feb. 2024.

[16] G. Chen, J. Si, R. Nie, J. Liang, and Y. Hu, "Analysis of armature magnetic field of slotless permanent magnet machine with arbitrary-phase equidirectional toroidal winding," *Energy Reports,* vol. 9, pp. 350-358, Apr. 2023.

[17] J. H. Park and S. G. Min, "Power-constrained design optimization of PM machines for low-power low-voltage and high-torque applications," *IEEE Transactions on Transportation Electrification,* pp. 1-1, 2023.

[18] X. Liang, M. Wang, P. Zheng, J. Gao, and W. Li, "Research and analysis of toroidal and conventional windings in permanent magnet synchronous

machine," in *IEEE International Magnetic Conference*, pp. 1-2, 2023.

[19] J. Si, T. Zhang, R. Nie, C. Gan, and Y. Hu, "Comparative study of dual-rotor slotless axial-flux permanent magnet machines with equidirectional toroidal and conventional concentrated windings," *IEEE Transactions on Industrial Electronics,* vol. 70, no. 2, pp. 1216-1228, Feb. 2023.

[20] Y. Wei, J. Si, Y. Han, Y. Li, and C. Gan, "Comparative analysis between slotless axial flux permanent magnet motor with equidirectional toroidal winding and integral-slot winding," *IEEJ Transactions on Electrical and Electronic Engineering,* vol. 17, no. 12, pp. 1790-1797, Dec. 2022.

[21] X. Chai, J. Si, Y. Hu, Y. Li, and D. Wang, "Characteristics analysis of double-sided permanent magnet linear synchronous motor with three-phase toroidal windings," *The Applied Computational Electromagnetics Society (ACES) Journal,* vol. 36, no. 8, pp. 1099-1107, Aug. 2021.

[22] Y. Wang, W. Zhang, R. Nie, J. Si, W. Cao, and Y. Li, "Analysis of a sinusoidal rotor segments axial flux interior permanent magnet synchronous motor with 120-degree phase belt toroidal windings," *The Applied Computational Electromagnetics Society (ACES) Journal,* vol. 37, no. 4, pp. 507-515, Apr. 2022.

[23] C. Gao, M. Gao, J. Si, Y. Hu, and C. Gan, "A novel direct-drive permanent magnet synchronous motor with toroidal windings," *Energies,* vol. 12, no. 3, Art. 432, Feb. 2019.

[24] J. K. Si, T. X. Zhang, Y. H. Hu, C. Gan, and Y. S. Li, "An axial-flux dual-rotor slotless permanent magnet motor with novel equidirectional toroidal winding," *IEEE Transactions on Energy Conversion,* vol. 37, no. 3, pp. 1752-1763, Sep. 2022.

[25] F. Xu, T. R. He, Z. Q. Zhu, Y. Wang, S. Cai, H. Bin, D. Wu, L. M. Gong, and J. T. Chen, "Influence of slot number on electromagnetic performance of 2-pole high-speed permanent magnet motors with toroidal windings," *IEEE Transactions on Industry Applications,* vol. 57, no. 6, pp. 6023-6033, Nov. 2021.

[26] L. J. Wu, Z. Q. Zhu, D. Staton, M. Popescu, and D. Hawkins, "Analytical model of eddy current loss in windings of permanent-magnet machines accounting for load," *IEEE Transactions on Magnetics,* vol. 48, no. 7, pp. 2138-2151, July 2012.

[27] F. Xu, T. R. He, Z. Q. Zhu, Y. Wang, S. Cai, H. Bin, D. Wu, L. M. Gong and J. T. Chen, "Influence of slot number on electromagnetic performance of 2-pole high-speed permanent magnet motors with toroidal windings," *Fifteenth International Conference on Ecological Vehicles and Renewable Energies (EVER)*, pp. 7, 2020.

[28] J. T. Chen and Z. Q. Zhu, "Comparison of all- and alternate-poles-wound flux-switching PM machines having different stator and rotor pole numbers," *IEEE Transactions on Industry Applications,* vol. 46, no. 4, pp. 1406-1415, July-Aug. 2010.

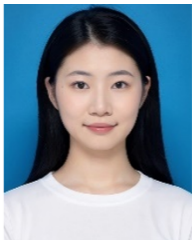

Yinjun Sun was born in Nanyang, Henan, China. She received B.S. degree in electrical engineering and automation from Xuzhou University of Technology, Xuzhou, China, in 2022. She is currently pursuing the M.S. degree with the College of Electrical Engineering of Zhengzhou University, Zhengzhou, Henan, China. Her current research interests include design, analysis and control of high-speed permanent magnet motors.

Peixin Wang received the B.Sc. and M.Sc. degrees from the School of Electrical Engineering and Automation, Henan Polytechnic University, Jiaozuo, China, in 2016 and 2018, respectively, and the Ph.D. degree from the Department of Electrical Engineering, Southeast University, Nanjing, China, in 2022. Since 2023, he has joined the School of Electrical and Information Engineering, Zhengzhou University as a research fellow. His research interests include permanent magnet and 2DoF machine systems.

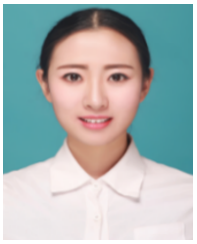

Rui Nie received the B.S. degree in electrical engineering from Henan Polytechnic University, Jiaozuo, China, in 2015, and the Ph.D. degree in electrical engineering from the China University of Mining and Technology, Xuzhou, China, in 2020. She is currently a Post-Doctoral Researcher with the School of Electrical and Information Engineering, Zhengzhou University. Her current research interests include linear motor design and control, and renewable energy generation technology.

Fuquan Nie received the B.S. degree in mechanical and electrical from Henan Institute of Science and Technology, Xinxiang, China, and the M.S. degree from Henan University of Science and Technology, Luoyang, China. He is currently Dean of the mechanical and electrical department of Henan Institute of Science and Technology. He has authored and co-authored over 400 technical articles. His main research interests include the theory, application, and control of the crane. He was named the national ten thousand program leading talents, national innovation talents promotion project of science and technology innovation talents.

Peng Gao received B.S. degree in electrical engineering and automation from Zhengzhou University, Zhengzhou, China, in 2014. He works in Henan United Electric Power Technology Co. Ltd., Zhengzhou, China. He engages in grid source coordination, power engineering debugging and transformation, thermal control professional technical supervision.

Jikai Si received the B.S. degree in electrical engineering and automation from the Jiaozuo Institute of Technology, Jizaozuo, China, in 1998, the M.S. degree in electrical engineering from Henan Polytechnic University, Jizaozuo, in 2005, and the Ph.D. degree from the School of Information and Electrical Engineering, China University of Mining and Technology, Xuzhou, China, in 2008. He is currently a Distinguished Professor with Zhengzhou University, Zhengzhou, China. He has authored and co-authored over 160 technical articles. His main research interests include the theory, application, and control of special motor. Prof. Si is a member of the Green Motor System Professional Committee, China.